Journal of Magnetic Resonance 301 (2019) 10–18

Contents lists available at ScienceDirect

Journal of Magnetic Resonance

journal homepage: www.elsevier.com/locate/jmr

Orientational dependencies of dynamics and relaxation of multiple quantum NMR coherences in one-dimensional systems

G.A. Bochkin [a], E.B. Fel'dman [a], I.D. Lazarev [a,b], A.A. Samoilenko [a], S.G. Vasil'ev [a,*]

[a] Institute of Problems of Chemical Physics of Russian Academy of Sciences, Chernogolovka, Moscow Region 142432, Russia
[b] Faculty of Fundamental Physical-Chemical Engineering, Lomonosov Moscow State University, GSP-1, Moscow 119991, Russia

ARTICLE INFO

Article history:
Received 10 November 2018
Revised 25 February 2019
Accepted 26 February 2019
Available online 27 February 2019

Keywords:
Multiple-quantum NMR
One-dimensional spin systems
Spin dynamics
Relaxation
Angular dependence

ABSTRACT

Dynamics and relaxation, or decoherence, of multiple quantum (MQ) coherences are investigated experimentally and theoretically for different orientations of a single crystal of fluorapatite with respect to the external magnetic field. Dynamics of MQ coherences is studied as a function of the preparation period of the MQ NMR experiment. Their relaxation, or decoherence, during the evolution period is also investigated. Universal curves for dynamics and relaxation are obtained and describe the experimental data for different orientations of the investigated sample. Those curves prove the dipolar nature of the observed relaxation process. The contribution of the heteronuclear interactions to the dipolar relaxation is also investigated. The source of discrepancies between experimental data and theoretical results in the experiments with a large angle between the nuclear spin chains and the external magnetic field are discussed.

1. Introduction

The opportunities of exploitation of quantum mechanical systems for information processing have been studied extensively over the recent years. Nuclear spins provide an attractive and insightful model for qubits owing to good isolation from the environment and wide opportunities to manipulate spin system by radiofrequency electromagnetic fields [1–3]. In particular, spin-1/2 nuclei exhibit a simple two-state structure of qubits and are well isolated from the environment. The latter feature is expected to ensure long coherence times and hence allow for a large number of logic operations in a quantum device to be performed. Useful implementations in quantum information processing require the preparation and control of multi-qubit states on large quantum registers consisting of thousands of highly correlated qubits [4,5]. Solid crystal devices hold promise for the scalable implementations [2,3]. The interactions of the system of qubits with the environment degrade quantum correlations. This process, known as decoherence, is usually considered the main obstacle in the implementation of quantum devices [4–6]. Thus, the understanding of the decoherence process is of great importance. Multiple quantum (MQ) NMR [7] is of special interest in the investigation of multi-qubit coherent states since it allows the creation of such states for a large number of $I = 1/2$ spins, interacting through the magnetic dipole-dipole interaction (DDI), and the observation of their relaxation due to the action of a correlated spin reservoir [5,6,8–10]. It is also worth noting that MQ NMR is very helpful for investigating main concepts of quantum information theory such as concurrence, entanglement, and quantum discord [11].

Among different physical implementations of quantum devices, spin chains have advantages from both practical and theoretical perspectives. Some proposals exist in the literature [12,13] to use spin-1/2 nuclei as qubits in relatively isolated atomic chains. The interaction between the spins is the magnetic dipole-dipole coupling. The regularity of the lattice creates identical local magnetic fields for the nuclei throughout the crystal and allows addressing the nuclei within each chain with a large magnetic field gradient. One-dimensional spin systems are beneficial in the theoretical studies of dynamics and relaxation in MQ NMR experiments since they provide the means of obtaining exact solutions. At present, a consistent quantum mechanical theory of MQ NMR dynamics had been developed only for one-dimensional systems [14,15], although many semi-phenomenological approaches in higher-dimensional systems have been proposed (for example, [16]). A well-known physical example of a one-dimensional chain of nuclear spins is a crystal of fluorapatite $Ca_5(PO_4)_3F$ (FAp). Distinctive features of ^{19}F NMR spectra lineshapes in a single-crystal of fluorapatite (FAp) has been recognized in early NMR experiments [17–19].

FAp is a hexagonal crystal with the space group $P6_3/m$ and the lattice parameters $a = 9.367(1)$ Å and c (the hexagonal axis)

* Corresponding author.
E-mail address: viesssw@mail.ru (S.G. Vasil'ev).

https://doi.org/10.1016/j.jmr.2019.02.004
1090-7807/

= 6.884(1) Å with one formula unit of $Ca_{10}(PO_4)_6F_2$ per unit cell [20]. The structure contains parallel chains of F ions along the *c*-axis of the crystal. The distance between neighboring chains is about three times greater than the distance between the nearest ions in a chain. Such an arrangement of the ^{19}F spins results in 40 times stronger dipolar coupling between the nearest spins in the chain than the strongest interaction with the spins of the neighboring chains. The calculated contribution to the second moment from ^{19}F spins within a chain is about 97% of the total second moment [17,18]. It is also significant that the strength of the dipolar interaction for a fixed angle θ decreases with the inverse cube of the distance and thus the dipole-dipole interaction of the next nearest neighbors is eight times weaker than the interactions of the nearest neighbors. The isolated spin chain with the nearest neighbor interactions is the basis of the theory of MQ NMR dynamics of one-dimensional systems [14,15,21]. The experimental studies of MQ NMR dynamics of one-dimensional systems were started in [22–24]. Our experimental results (Sections 5 and 6) are well described by the isolated chain model.

According to theoretical predictions, only MQ NMR coherences of orders 0 and ±2 arise in a one-dimensional spin chain initially prepared in the thermodynamic equilibrium state in the admittedly unrealistic approximation of exclusively nearest neighbor interactions [14,15,21]. Dynamics of those MQ coherences is usually investigated as a function of the duration of the preparation period of the MQ NMR experiment [7] when the external magnetic field is directed along the chain [25,26]. In this case, the interactions of spins from different chains are weak. We note that heteronuclear interactions are averaged by a pulse sequence irradiating the spin system on the preparation period. The strength of the dipolar coupling is responsible for the number of spins in the correlated cluster created in the MQ experiment [5,6,27,28] and affects the rate of their relaxation [5,9,27,28]. The specific arrangement of the spins in a linear chain allows "tuning" the dipolar coupling between the spins at will by the adjustment of the angle between the external magnetic field and the chain.

The peculiarities of the decay of the MQ NMR coherences during the evolution period of the MQ NMR experiment were discussed in the literature [6,9,29–31]. This period follows immediately after the evolution period. The DDI is responsible for the relaxation of the MQ NMR coherences, as we will demonstrate. The effect of inter-chain and heteronuclear interactions on the relaxation is small when the external field is directed along the chain. On the contrary, if the chain is at the "magic" angle with the external field [32], then the effect of these interactions can be very significant.

It should be noted that the dipolar relaxation considered in this article is a reversible process. The reversal can be achieved by using magic-sandwich echo [33]. It is possible that the term "dephasing" would be more suitable. We use the term "dipolar relaxation (or decay) of MQ coherences", as was done in the previous works [6,30,31].

In [34], the MQ NMR dynamics of a quasi-1D chain in a fluorapatite crystal was investigated in detail, both experimentally and numerically. The authors investigated the influence of defects in producing distributions of run lengths, and the contribution of interactions of the next nearest neighbors (NNN) for MQ NMR coherences. They showed that for durations of the preparation period of less than 0.5 ms the dynamics of the system is well described by a model with NN interactions. In our work we do not use the preparation period times more than 0.8 ms. The authors considered the so-called random cluster model [24] for an estimation of chain length distribution. The results in [34] were obtained for a single orientation only. A detailed analysis of the orientational dependence of MQ NMR coherences was not performed. In [24], MQ NMR coherences were investigated for two different crystal orientations. It is worth noting that in [24,34] no investigations of relaxation, or decoherence, of MQ NMR coherences were performed.

The paper is organized as follows. In Section 2 the experimental methods used for the investigation of the orientational dependencies of the dynamics and relaxation of MQ NMR coherences are described. The features of the crystal structure of FAp, relevant to NMR experiments, are described in Section 3. In Section 4, the orientation dependencies of ^{19}F NMR frequency and linewidth are presented. In Section 5, we investigate experimentally and theoretically the dynamics of the MQ coherences of order 0 and ±2 on the preparation period for different orientations of the sample relative to the external magnetic field. The orientational dependence of the relaxation time of the MQ NMR coherence of the second order on the evolution period is studied in Section 6. A summary is given in Section 7.

2. Experimental details

The experiments were performed on a Bruker Avance III spectrometer with the static magnetic field of 9.4 T (the corresponding frequency on ^{19}F nuclei is 376.6 MHz). A probe with a solenoid coil for 2.5 mm o.d. NMR sample tubes was used. The orientation of the sample with respect to the external magnetic field was achieved by the rotation of the sample tube around the solenoid axis. The duration of the $\pi/2$ pulses was $t_p = 0.8$ μs. The accuracy of the rotation was estimated to be 2°. The chemical shift values are reported relative to $CFCl_3$. Hexafluorobenzene (C_6F_6) at −160 ppm was used as an external reference.

MQ NMR experiments have been carried out using a conventional phase incremented even-order selective pulse sequence [7,35]. The scheme of the MQ NMR experiment includes four main periods: preparation (τ), free evolution (t), mixing (τ), and detection as shown in Fig. 1. MQ coherences are created on the preparation period by a proper pulse sequence which produces an average two-spin/two-quantum XY Hamiltonian. The basic cycle of the MQ NMR experiment consists of eight $\pi/2$ pulses of the duration t_p separated by the delays Δ and $\Delta' = 2\Delta + t_p$. The desired time of excitation of the MQ NMR coherences is accomplished by m repetitions of this cycle with the overall duration $\tau = 12m(\Delta + t_p)$.

Different durations of the preparation period were achieved by varying the delays Δ in the range of 0.8–2.5 μs and the number of basic cycles in the range of 1–22. The variation of these parameters resulted in the duration of the basic cycles in the range of 19.2–39.6 μs. The longest preparation time $\tau \approx 0.8$ ms. The intensities of the MQ NMR coherences at different durations of the free evolution period t were obtained in separate experiments. The recycle delay (RD) of 25 s was chosen in order to satisfy the condition $RD > 5T_1$ according to inversion-recovery measurements.

3. Sample description

The sample of natural FAp used in the investigation was from Irkutsk Oblast (Russia) and was translucent pale green. The initial crystal was a well-shaped hexagonal prism elongated along the *c*-axis. The crystal was cut to fit the dimensions of the 2.5 mm o.d. NMR tube. The dimensions of the crystal were approximately 3.8 × 1.5 × 1.5 mm. The orientation of the *c*-axis was perpendicular to larger faces of the sample. The ^{19}F NMR chemical shift, MQ coherence intensities, and relaxation were measured as functions of the crystal orientation. The rotation of the crystal was performed about an axis perpendicular to the *c*-axis of the crystal which was initially oriented along the external magnetic field (an arbitrary axis in the *ab*-plane of the crystal).

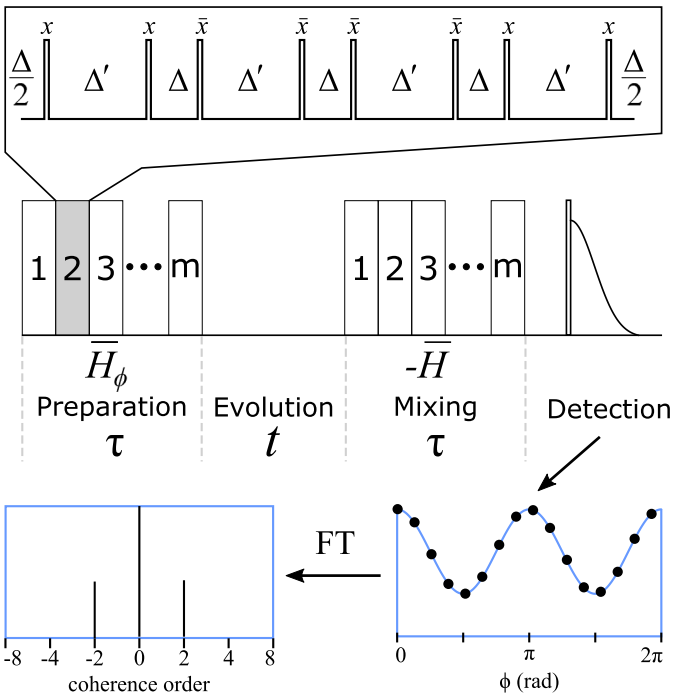

Fig. 1. Schematic representation of the pulse sequence of the MQ NMR experiment. MQ NMR coherences are created during the preparation period under the action of a series of m 8-pulse subcycles during the time τ and then converted back to observable magnetization after an identical (except for the 90 degree phase shift) mixing period [7,35]. The magnetization is then detected by the $\pi/2$ pulse. To separate the multiple-quantum orders, the relative phase ϕ between the preparation and mixing periods is incremented. The Fourier transform with respect to ϕ yields the MQ NMR spectrum. The intensities of the MQ NMR coherences at different times t of free evolution were obtained in separate experiments.

The structure of calcium fluorapatite is known from the single-crystal X-ray diffraction studies[20] and is shown in Fig. 2 (images were prepared using VESTA software[36]). FAp is a hexagonal crystal with the space group $P6_3/m$ and the lattice parameters $a = 9.367(1)$ Å and $c = 6.884(1)$ Å (the hexagonal axis) with one formula unit of $Ca_{10}(PO_4)_6F_2$ per unit cell. There are seven crystallographically inequivalent atomic sites in a unit cell (Fig. 2a). The F nuclei are arranged in linear chains along the c axis on the edges of the unit cells (Fig. 2). These nuclei are separated by the 1/2 of a c lattice spacing (3.44 Å) at the positions z = 1/4 and 3/4. Sixfold rotation axes passing through the corners of the unit cells result in the six nearest F^- ions at the distance of 9.37 Å in the plane perpendicular to the c-axis. It is known that there are two types of calcium ions in the structure, four CaI and six CaII. There are columns of Ca^{2+} ions which are parallel to the F nuclei chains and are separated from those chains by one half of the c-axis parameter. This accounts for two fifths of the Ca^{2+} ions in the crystal. These ions are given the designation CaI. The remaining Ca^{2+} sites, designated as CaII, form vertices of equilateral triangles in the plane perpendicular to the c-axis. The centers of the triangles are occupied by F^- ions. The distance between CaII and F^- ions is 2.34 Å. There are two triangles rotated by 60° from each other about the c axis. This constrains the c axis to threefold rotation symmetry. PO_4^{3-} tetrahedra are slightly distorted. This results in 3 inequivalent oxygen sites. The arrangement of P can also be described as equilateral triangles, staggered along the c-axis, in the plane perpendicular to the c-axis at the $z = 1/4$ and 3/4 positions with F^- ions in the center (Fig. 2a). The distance between F and the nearest P nuclei is 3.67 Å.

4. The orientation dependence of ^{19}F NMR chemical shift and lineshape in fluorapatite

The ^{19}F NMR absorption line of the FAp is known to be strongly anisotropic [17,18,37]. The variation of the angle between the c axis of the crystal and the external magnetic field results in changes of the position as well as the width of the line. The spectra recorded after a single $\pi/2$ pulse at different orientations of the sample with respect to the external magnetic field are shown in Fig. 3. The angle θ is defined as the angle between the external magnetic field and the crystal axis c. The ^{19}F chemical shift of the fluoride anion is very sensitive to the cations to which it is bound [37–39]. The orientation with respect to the external magnetic field of the CaII triangles around F^- ions strongly affects the ^{19}F chemical shift. The parallel orientation of the ^{19}F spin chains results in the most deshielded position of the line while the

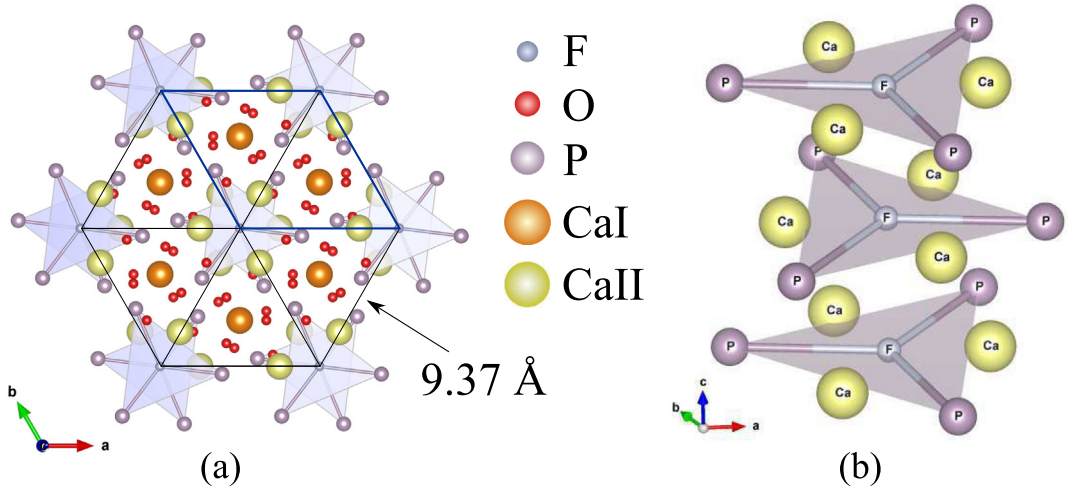

Fig. 2. (a) Fluorapatite structure viewed down the c-axis. One unit cell is highlighted. Every chain of ^{19}F nuclei running down the c-axis is surrounded by six identical chains at the distance of a lattice spacing $a = 9.37$ Å. (b) Part of the crystal structure of FAp showing the surroundings of the fluorine atoms. Oxygen atoms have been removed for clarity. Fluorine atoms are equally spaced ($r_{FF} = 3.44$ Å) and arranged in columns along the c-axis of the crystal. Every fluorine atom is surrounded by three equidistant phosphorus atoms at $r_{FP} = 3.67$ Å situated in the vertexes of equilateral triangles in the planes perpendicular to the c-axis as well as by three CaII ions at the distance of 2.34 Å.

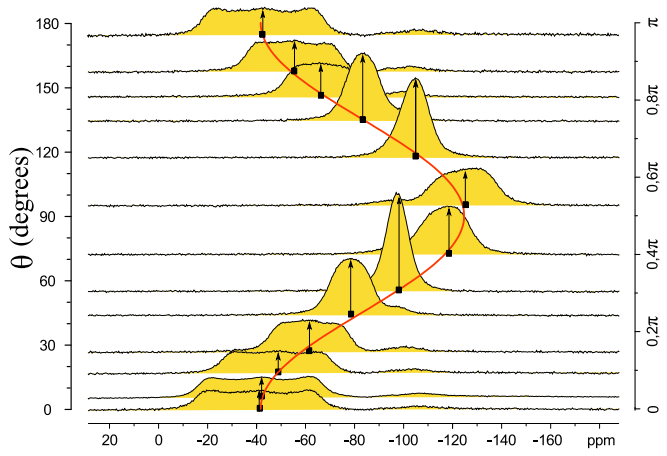

Fig. 3. The changes of the ^{19}F NMR spectra of FAp due to the rotation of the crystal *c*-axis about an axis perpendicular to the external magnetic field.

perpendicular orientation shows the biggest upfield shift. The chemical shift of the FAp is known to be axially symmetric [23,37–39]. This is well supported by our experiments. The following convention for the chemical shift tensor components is used [32]:

$$|\delta_{11} - \delta_{iso}| \leqslant |\delta_{22} - \delta_{iso}| \leqslant |\delta_{33} - \delta_{iso}| \quad (1)$$

where δ_{ii} ($i = 1,\ 2$ or 3) are the components of the tensor in the direction of the principal axes in the molecular framework, $\delta_{iso} = \frac{1}{3}(\delta_{11} + \delta_{22} + \delta_{33})$ is the isotropic chemical shift. For the case of an axially symmetric chemical shift tensor one expects the following dependence on the angle θ [37,40]:

$$\delta = \delta_{\perp} \sin^2\theta + \delta_{\parallel} \cos^2\theta = \delta_{\perp} + \Delta\delta \cos^2\theta, \quad (2)$$

where δ is the effective chemical shift, $\delta_{\perp} = \delta_{11} = \delta_{22}$ and $\delta_{\parallel} = \delta_{33}$ are components of the tensor, and $\Delta\delta = (\delta_{\parallel} - \delta_{\perp})$ is the chemical shift anisotropy.

The evolution of the ^{19}F NMR spectra with the rotation of the FAp crystal about an axis perpendicular to the external magnetic field is shown in Fig. 3. The chemical shift anisotropy parameters were determined using Eq. (2). The obtained parameters $\delta_{iso} = -97 \pm 1$ ppm and $\Delta\delta = 87 \pm 1.5$ ppm are in close agreement with the data reported for mineral FAp in the literature [37–39,41]. The chemical shift dependence was used as the reference for the determination of the angle between the spin chains and the external magnetic field. In the consideration of the dipolar interactions, the most relevant nuclei in FAp are ^{19}F and ^{31}P. These nuclei are spin-1/2 isotopes with high gyromagnetic ratio and 100% natural abundance. The remaining nuclei in the structure could be safely ignored due to low content of NMR active isotopes and their low gyromagnetic ratios, namely ^{43}Ca ($I = 7/2$, natural abundance 0.045%) and ^{17}O ($I = 5/2$, natural abundance 0.037%).

The secular Hamiltonian of the dipole-dipole interaction can be written as

$$H_{dz} = \sum_{i<j} D_{ij}\left(3I_i^z I_j^z - \mathbf{I}_i \cdot \mathbf{I}_j\right) = \sum_{i<j} D_{ij}\left[2I_i^z I_j^z - \frac{1}{2}\left(I_i^+ I_j^- + I_i^- I_j^+\right)\right], \quad (3)$$

where I_m^{α} is the α-projection ($\alpha = x; y; z$) of the spin angular momentum operator, I_m^+ and I_m^- are the raising and lowering operators of spin m, respectively, $\mathbf{I}_i \cdot \mathbf{I}_j = I_i^x I_j^x + I_i^y I_j^y + I_i^z I_j^z$, and D_{ij} is the dipolar coupling constant between spins i and j:

$$D_{ij} = \frac{\gamma^2\hbar}{2r_{ij}^3}\left(1 - 3\cos^2\theta\right) = b_{ij}\left(1 - 3\cos^2\theta\right) \quad (4)$$

When the orientation of the chains is parallel to the orientation of the external magnetic field the resonance is symmetrically split up into three lines. The line shape could be roughly interpreted as the splitting of the resonance due to the two nearest neighboring spins. The splitting due to a single nearby spin amounts to 6*b*. This value is equal to the highest possible splitting for the dipolar pair [42]. Taking into account the identical interaction with another neighboring spin we obtain the triplet with the spacing of the outer pair of lines of 12*b* and the relative intensities of the components 1:2:1 [17]. More accurate calculations for the infinite evenly spaced spins arranged in a linear chain take into account all nearest and the next nearest neighbor interactions and lead to a complex multiplet pattern [18]. A detailed fine-structure of the splitting is masked by other line-broadening interactions such as interactions between spin chains, interactions with far neighbors along a spin chain, and heteronuclear interactions, but the distinctive triplet structure is conserved [17,18]. This pattern could be roughly described as the triplet with the splitting of the adjacent lines of about 6*b* and more even intensity distribution among the lines.

The experimentally observed pattern could be almost equally well approximated by 3 equal Gaussian peaks (intensities 1:1:1) or by a broader resonance at the center and two identical satellites with smaller intensities and widths (intensities 1:2:1). For the distance between the nearest fluorine spins of 344 pm, the value of $b = 8.217 \times 10^3\ \mathrm{s}^{-1} = 2\pi \times 1.308$ kHz. The experimentally observed splitting of the outer lines of the triplet (15.7 ± 0.4 kHz) is in excellent agreement with value calculated from the structural data ($12b = 15.7$ kHz). The effect of the FAp crystal rotation about an axis perpendicular to the *c* axis on the chemical shift and the line width in ^{19}F NMR spectra is summarized in Fig. 4. The line width measured at the half maxima in ^{19}F spectra of FAp has the same angular dependence as that for a rigid pair of identical nuclei [42].

$$\Delta\nu \sim |D_{ij}| \sim A|1 - 3\cos^2\theta|, \quad (5)$$

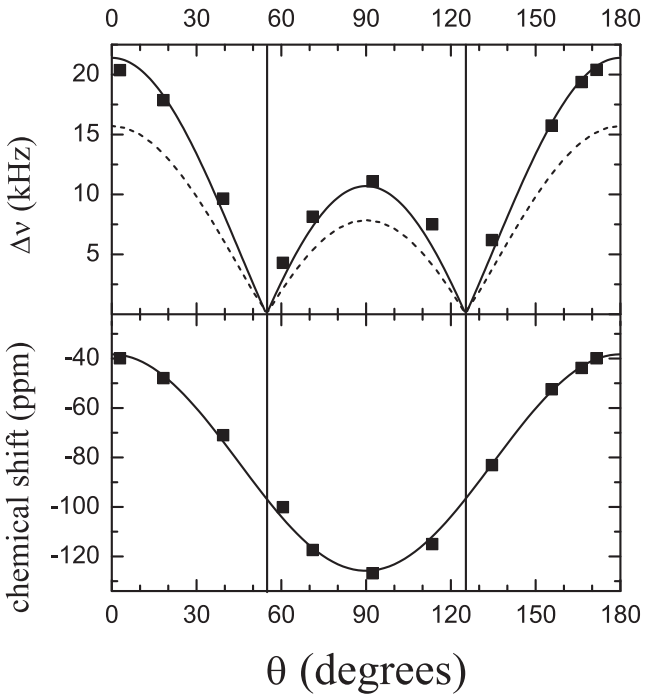

Fig. 4. The dependence of the line width (top) and the chemical shift (bottom; the data are identical to those of Fig. 3) on the angle θ for single-crystal FAp. The experimental data are shown by squares and the relevant analytical curves by solid lines. The dashed line corresponds to the expected splitting of the outer lines in the triplet.

where A is a constant. The approximation of the experimental data with $A = 10.7$ kHz in Eq. (5) is shown in Fig. 4 with the solid line. The expected splitting of the outer lines in the triplet which have the functional form of Eq. (5) with $A = 6b = 7.86$ kHz is represented by the dashed line. When the c-axis of the crystal is rotated away from the direction of the magnetic field, the fine structure gradually disappears (Fig. 3). The satellites become unresolved for the angles above approximately 30 degrees off the magnetic field.

5. Orientational dependencies of intensities of MQ NMR coherences in one-dimensional chains

The developed theory of MQ NMR dynamics of one-dimensional chains [14,15,21] allows us to calculate the intensities of MQ coherences of orders 0 and ±2 on the preparation period of the MQ NMR experiment [7]. The theory gives an exact solution in the approximation of the nearest-neighbor interactions between spins. The solution is valid for relatively small preparation times. In particular, there exist very simple expressions for the intensities of MQ coherences [14,15,21] in the case of long linear spin chains (with the number of spins $N \gg 1$):

$$G_0(\tau) = \frac{1}{2} + \frac{1}{2}J_0(4D\tau), \tag{6}$$

$$G_{\pm 2}(\tau) = \frac{1}{4} - \frac{1}{4}J_0(4D\tau), \tag{7}$$

where τ is the length of the preparation period, $D = D_{i,i+1}$ is the dipolar coupling constant of the nearest neighbors, and J_0 is the Bessel function of the first kind of order 0.

Taking into account that the only argument affecting the evolution of MQ NMR coherences in Eqs. (6 and 7) is $4D\tau$, the dependence of MQ NMR coherence intensities on the preparation period for different orientation of the spin chain can be generalized in a simple way by introducing the dimensionless scale factor $|D(\theta)/D(0)|$ for the preparation time τ. In other words, we introduce the scaled preparation time axis:

$$\overline{\tau} = \frac{|1 - 3\cos^2\theta|}{2}\tau, \tag{8}$$

for which MQ NMR coherence intensities of zero- and ±2 orders obtained at different orientations collapse onto a single master curve $G_0(\overline{\tau})$ and $G_{\pm 2}(\overline{\tau})$ correspondingly. The absolute value in the expression accounts for the fact that MQ coherence intensities are insensitive to the sign of the dipolar coupling constant, according to Eqs. (6 and 7).

In Fig. 5 the dependences of the intensities of the MQ coherences of orders 0 (upper part) and ±2 (lower part) on the scaled preparation time for different sample orientations are shown. Experimental values are shown as dots and the corresponding theoretical expressions (Eqs. (6 and 7)) are given by the solid lines. Theoretical curves were calculated for the parallel orientation of the crystal using the $D = 16.0 \times 10^3$ s^{-1} as in our previous publications [9,26–28]. This value is slightly less than the value expected from the structural data $D = 2b = 16.4 \times 10^3$ s^{-1} but falls within the margin of error.

The dipolar interaction constant determines the local fields due to the neighboring spins. For most of the experiments the cycle times of 19.2, 20.4 and 21.6 μs were used. Longer times were used only for the orientations close to the magic angle. One should emphasize that even one-quarter (two pulses) of the Baum-Pines pulse sequence, in principle, gives the DQ average Hamiltonian. For such a two-pulse part of the sequence (of length $\tilde{t}_c < 5$ μs), the condition $\omega_{loc}\tilde{t}_c < \frac{1}{12}$ holds in all our experiments ($\omega_{loc} \approx 1.6 \times 10^4$ s^{-1}). The full sequence is necessary for averaging

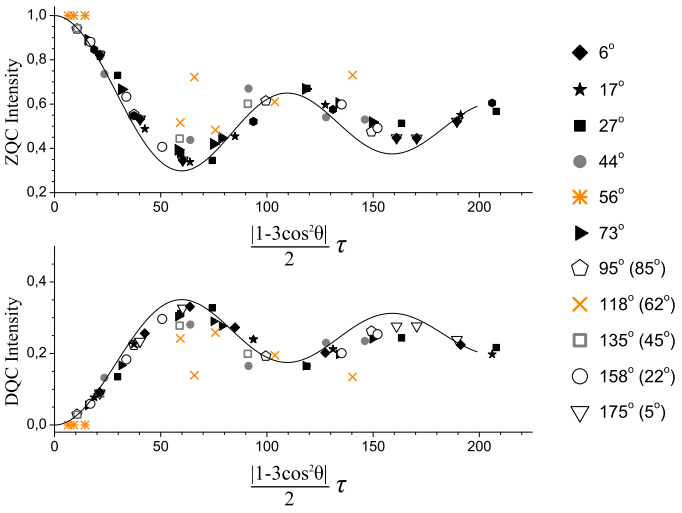

Fig. 5. The dependencies of the intensities of the MQ NMR coherences of orders 0 (top) and ±2 (bottom) on the scaled preparation time for different sample orientations.

other imperfections (for example, the effects of finite duration of the pulses).

Experimentally observed MQ NMR coherence intensities follow the theoretical predictions quite well in the considered range of the preparation times. Obvious deviations are observed only for the orientations close to the magic angles (56° and 118° in Fig. 5), where the dipolar coupling between the spins in the same chain becomes too small. For the orientation 56°, the emergence of the coherences of the ±2 orders was not observed. The MQ coherences for the orientation 118° are apparently due to the interactions of the spins in different chains and hence do not follow the common trend. Some small deviations are observed for the angles of 44° and 135° which are still close to the magic angle. The latter deviations could be ascribed to a larger influence of the angle setting error. The changes of the dipolar constant in this range are the biggest which result in a greater error in the determination of the correction factor for the preparation time. Orientations of the chain close to the perpendicular to the external magnetic field do not show significant deviations of the MQ intensities despite the fact that the intrachain dipolar coupling is reduced twice while the interchain coupling is maximal. Taking into account that the only adjustable parameter in the theory is the dipolar coupling constant between nearest neighbors in the chain, the data match the curve very well.

The first investigation of the MQ NMR dynamics in oriented crystals of fluorapatite was presented in [24]. Only two different orientations of the chains with respect to the external magnetic field were considered (62 and 90 degrees). It was revealed that the intensities of the zero- and two-quantum coherence orders plotted versus preparation time show oscillatory behavior. These data can be explicitly compared with the theory for the MQ dynamics of linear spin chains with nearest neighbor interactions [14] using the scaled time axes proposed in the present article. For this purpose, the original data of fig. 4 in [24] should be squeezed along the preparation time axis by a factor of 5.9 and 2 for the orientations of 62 and 90 degrees, respectively, according to Eq. 8. The data for 62° orientation showing the first minimum and maximum well correspond to the universal curve represented by the solid line in Fig. 5. The curves for 90° orientation were measured less accurate with respect to the "frequency" of the oscillations, however the positions of the maxima and minima appear to be reproduced by the universal curve. The intensities of the

two-quantum coherence orders are smaller than that obtained in our studies. This can be the consequence of the adverse effects of the higher-order terms in the average Hamiltonian of the pulse sequence since the durations of the pulses (4.6 μs) and the basic cycle of the sequence (78 μs) used in [24] were much longer than that used in the present investigation (0.8 and 20 μs, respectively).

The apatite structure is known to be very prone to a variety of anionic and cationic substitutions [20]. Natural fluorapatites could contain defects such as OH^- or Cl^- ions or vacancies replacing F^- ions in the columns. Even in pure single crystals, some defects interrupting the spin chain are expected to be present [43]. This results in finite-length segments of F spins in the structure rather than infinite spin chains. The effect of the finite lengths of the chains on the ^1H MQ NMR dynamics was investigated by Yesinowski and coauthors [22,24] on powdered samples of hydroxyapatites (OHAp) and fluorohydroxyapatites (FOHAp). Oscillatory behavior, typical for oriented linear chains [14,15,24], is not observed for the polycrystalline samples of apatites. Instead, a steady growth of the higher order MQ coherence orders is observed with the increasing preparation time. The dimensionality of spin distributions in solids has a strong influence on the growths of higher order coherences. 1D systems show much slower MQ growth compared to 2D systems which is in turn slower than that of 3D systems [44]. The growth rate of MQ NMR coherences is typically characterized by the growth exponent α in the power law dependence of the type $N \sim \tau^{\alpha}$, where N is the number of the correlated spins. The "effective size" N is extracted from the distribution of the intensities of MQ NMR coherences at a given preparation time according to the "Gaussian model" [7] by fitting the intensities $I(n)$ to a Gaussian function $\exp(-n^2/N)$, where n is the coherence order. It was found [22,24] that the growth exponent for a highly stoichiometric sample of OHAp is close to 1 ($\alpha = 0.98$), while a slight deficiency of hydroxyl groups in another sample of OHAp leads to a marked decrease in the growth exponent (α=0.83). Even smaller values were observed for FOHAp with the composition $Ca_5(PO_4)_3F_x(OH)_{1-x}$ with $x = 0.24$ ($\alpha = 0.57$) and $x = 0.41$ ($\alpha = 0.50$). In [45], the growth of the second moment of the MQ NMR intensity distribution was investigated, using the same experimental data.

To examine the possible influence of the non-ideal composition of the mineral crystal used in our study on the experimental results we have performed measurements of the growth rate. For the sake of comparison the sample was powdered. The usage of the same 8-pulse Baum-Pines MQ sequence [7,46] was inefficient (line-shape distortions and reduced amplitude) due to a considerable chemical shift range [23,47]. The performance of the sequence was substantially improved by addition of four 180° pulses for the offset compensation as proposed in [48]. We observed the MQ coherences up to the eighth order. The MQ coherences of the orders higher than 2 appear at later preparation times in comparison with polycrystalline OHAp. This agrees with the literature [23,43]. The number N of the correlated spins was obtained by least-squares fitting of the orders of coherence (excluding the zero-quantum coherence) to a Gaussian function [7,22,24] as discussed above. The results are shown in Fig. 6. Alternatively the problems arising due to the wide chemical shift range can be resolved using the chemical-shift-selective MQ NMR pulse sequence [23]. In that case the carrier frequency is placed at the desired position in the powder spectrum while the homogeneously broadened peaks at all the other chemical shifts are saturated prior to the application of the MQ NMR pulse sequence.

The growth exponent is equal to 0.94 ± 0.05. This value is close to 1.0 which is expected for fluorapatite with high ^{19}F content. Additionally, we have performed a quantitative ^{19}F NMR analysis by comparing signals from known amounts of CaF_2 and FAp (both

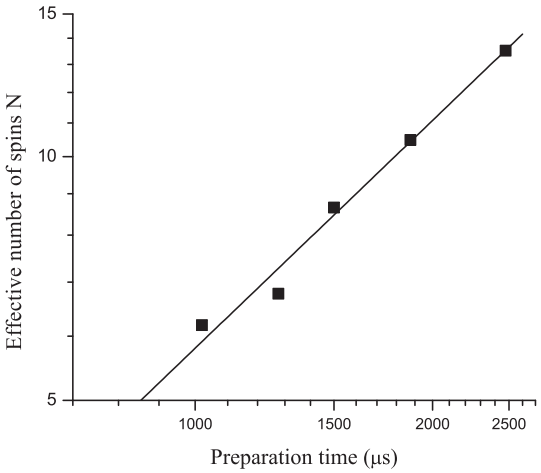

Fig. 6. The dependence of the effective number N of the correlated spins on the duration of preparation period of MQ NMR experiment τ for polycrystalline sample.

polycrystalline samples). The ^{19}F content in FAp was determined to be approximately $87 \pm 10\%$ of the stoichiometric ratio. We could not accurately determine the ^1H signal from our sample because it was of the same order of magnitude as the background though we avoided the proton-containing materials in the probe construction and the background is not a problem for other samples.

An additional confirmation of the absence of appreciable OH content in the sample comes from the line-shape analysis. If the external magnetic field is parallel to the c axis, the ^{19}F line shape for FAp is a poorly resolved triplet as discussed in Section 4. For protons, the line shape is practically the same as for the fluorine except for a larger separation of the triplet due to a larger gyromagnetic ratio [17,49]. The presence of OH defects in FAp results in the appearance of additional lines outside the triplet in ^{19}F spectra as it was shown for the sample with OH:F ≈ 1:5 [50]. For the OHAp sample containing a small amount of fluorine (F:OH ≈ 1:12) the ^{19}F spectrum consists of a triplet and a doublet [49].

Other substitutions in the structure of FAp, such as substitutions in Ca positions, can also affect the results of MQ experiments. Such substitutions should affect the chemical shift anisotropy of the neighboring ^{19}F nuclei. This was not observed in our experiments, as shown in Section 4. This result is confirmed by the EDX (energy dispersive X-ray) analysis, which shows the absence of the elements other than F, O, P, and Ca in the sample.

Relatively short T_1 values (3.8 s for parallel orientation and 5 s for the orientation close to the magic angle) for our sample in comparison with chemically pure synthetic crystals ($T_1 = 1100$ s was observed for the parallel orientation in [43] and 91 s for a powdered sample in [23]) show the presence of sparse paramagnetic impurities. This time scale is many orders of magnitude greater than the time scales explored in MQ experiments. According to the data presented above, the sample contains an acceptable degree of non-ideality in the 1D chain and this does not strongly affect the experimental results.

6. Orientational dependence of the relaxation time of the MQ NMR coherence of order 2

Our calculations show that, when the ^{19}F chains are parallel to the external magnetic field, the heteronuclear interactions do not significantly contribute to the relaxation of the MQ NMR coherences (their contribution to the second moment of the line shape

of the MQ coherence of order 2 is about 5% of the total for small τ, less for large τ), but for some other orientations their effect can be significant.

The calculation of the relaxation time is performed numerically for a chain of $N = 16$ spins. The length of 16 spins was chosen because it was the maximum for which calculations could be performed on the computer used. The results for 12 spins are not substantially different (the difference in relaxation time is less than 2 μs for the preparation period lengths shown in Figs. 5 and 7). This shows that the presence of occasional defects splitting the spin chain into fragments (discussed in the previous section) should not have a significant effect on our results, given the time scales in our experiments. We will denote the intensity of order-2 MQ coherence after the preparation period of the length τ and the evolution period of the length t as $F_2(\tau, t)$. We take the exact solution for the dynamics of a quasi-one-dimensional spin chain (with nearest-neighbor couplings) on the preparation period [21] as the initial condition. In the case of chains parallel to the external magnetic field, the dipolar coupling constant between the nearest neighbors in a chain is about 40 times greater than the dipolar coupling constant between spins in different chains. Such an approach is not applicable in the case of chains forming an angle close to the magic angle ($\theta = \arctan\sqrt{2} \approx 54.74^\circ$) with respect to the external magnetic field, because the chains can no longer be considered as quasi-one-dimensional. We use the following criterion to determine the significance of the inter-chain interactions:

$$\sum_q D_{qi}^2 < 5 \cdot \left(2D_{NN}^2\right), \tag{9}$$

where q can be any spin from chains adjacent to the chain to which the spin i belongs, D_{NN} is the nearest-neighbor dipolar interaction constant, D_{qi} is the dipolar constant between spins q and i. This means that the theory is inapplicable in the interval $47^\circ < \theta < 64^\circ$ (and $116^\circ < \theta < 133^\circ$). Otherwise, the inter-chain interaction on the preparation period is neglected.

The pulse sequence [7,46] used to generate MQ NMR coherences averages the heteronuclear dipolar couplings to zero during the preparation period. However, these couplings are important on the evolution period since they affect the relaxation rates of the ^{19}F MQ NMR coherences.

The intensity of the MQ NMR coherence of the second order decays faster than that of the zeroth-order [9]. Besides, it turned out that the relaxation of the MQ NMR coherence of the second order can be considered as a model of decoherence of a many-qubit cluster in a one-dimensional spin chain [27]. Below we consider the decay of that coherence.

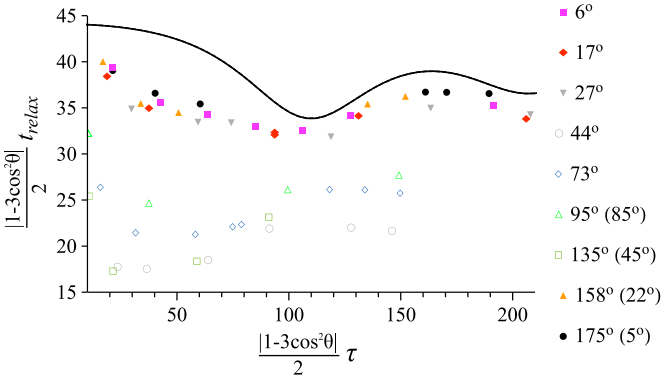

Fig. 7. The dependencies of the scaled relaxation times of the MQ NMR coherence of order 2 on the scaled duration of the preparation period for different sample orientations. The experimental results are shown with dots and the numerical calculation for the chain consisting of 16 spins are shown with a solid line.

The decay of the intensity of the MQ NMR coherences of the second order on the evolution period can be approximated with the Gaussian function [9]:

$$\widetilde{F}_2(\tau, t) = F_2(\tau, 0) e^{-M_2^{(2)} \frac{t^2}{2}}, \tag{10}$$

where $M_2^{(2)}$ is the second moment of the line shape of the MQ coherence of the second order. This semi-phenomenological formula agrees well with the experimental data. It is easy to see that according to Eq. (10), the relaxation rate of the order-2 MQ coherence is determined solely by the second moment, which determines the characteristic time scale of relaxation. We define the relaxation time as the time when the approximated intensity $\widetilde{F}_2(\tau, t)$ decreases to $1/e$ of its value at the start of the evolution period. Thus, the relaxation time of the order-2 MQ coherence is calculated from the second moment as follows:

$$T_{relax} = \sqrt{\frac{2}{M_2^{(2)}}}. \tag{11}$$

As regards the order-0 MQ coherence, the definition of its relaxation time is complicated by the fact that it does not decay to zero on the evolution period, but reaches a stationary value (which can be larger than $1/e$ times the initial value) [9]. The formula (10) has to be modified to account for that. Thus, studying the relaxation of the order-2 coherence is methodically clearer.

The calculation of the second moments is similar to [51]: we take the exact solution of the dynamics of the system on the preparation period, and calculate the second moment using the formula [29]:

$$M_2^{(2)} = \frac{\mathrm{Tr}\{[\rho_2(\tau), H][H, \rho_{-2}(\tau)]\}}{N 2^{N-2} F_2(\tau, 0)}, \tag{12}$$

where ρ_2 is the part of the density matrix of the system describing the second-order MQ coherence at the end of the preparation period, and H is the Hamiltonian governing the system during the evolution period. A numerical calculation for a chain with $N = 16$ spins shows that the introduction of interactions between remote nuclear spins on the same chain on the evolution period improves the agreement with the experiment. Unfortunately, analytical calculations in that case are very cumbersome; therefore, we restrict ourselves to numerical ones. This necessitates using the exact solution for a finite chain (with nearest-neighbor couplings) from [21] rather than for an infinite chain [14,15] as in [51].

In order to present the experimental and theoretical results for the spin relaxation time for different sample orientations, we introduce the scaled relaxation time, analogously to the scaled preparation time (Eq. (8)):

$$\overline{T}_{relax}(\theta) = \frac{|1 - 3\cos^2(\theta)|}{2} T_{relax} \tag{13}$$

In Fig. 7 the dependencies of the scaled relaxation times of the MQ NMR coherences of the second order on the scaled lengths of the preparation period are given for different orientations of the sample.

As might be expected, the theoretical predictions yield good agreement with the experimental data when the orientation of the chains is close to the orientation of the external magnetic field. However, at the orientations which approach the limits of the theory as defined by Eq. (9) the experimental relaxation rates are significantly faster than the calculated values. The shortest relaxation times are observed for the angles 44° and 135°. As was discussed in the previous section, these orientations are located in the range where the variation of the dipolar coupling constant with respect to a change in the angle θ is large. Nevertheless, such discrepancies cannot be exclusively ascribed to the error in the angle settings.

The relaxation rates measured at these two different orientations show a similar trend. Moreover, the orientations at 73° and 95° which lie between the magic angles and close to the perpendicular orientation also show faster, though less pronounced, relaxation rates. For this range of the orientations, the change of the dipolar coupling with the angle is significantly smaller. Consequently, these notable differences are not associated with the accuracy of the angle setting.

The observed discrepancies can be attributed to the increasing influence of the dipolar coupling between spins belonging to different chains. Approaching the chain orientation close to perpendicular to the magnetic field direction results in the increase of both the dipolar coupling between spins of different chains and surrounding ^{31}P spins while the intrachain dipolar couplings are significantly reduced.

In contrast to the dependences of the intensities, where the experimental data are consistent with the theory in the whole range of the angles except for the close vicinity of the magic angles, the relaxation times conform to the theory's predictions within a narrower range of approximately 30° around the parallel orientation. This range roughly corresponds to the orientations where the splitting due to the nearest neighbors is resolvable in the single quantum spectra (see Fig. 3). The theory gives quite a good prediction of the experimental data in spite of the fact that the intrachain dipolar interactions decreases to 1.6 times the value for the parallel orientation on the boundary of this range and the interchain and heteronuclear dipolar interactions become more significant.

7. Conclusion

We investigated experimentally and theoretically the dynamics and relaxation of the MQ NMR coherences for different sample orientations relative to the external magnetic field on quasi-one-dimensional system of fluorine spins in fluorapatite. We have shown that the effect of inter-chain and heteronuclear interactions on the relaxation time can be significant for some orientations of the sample. The experimental data on the dynamics and relaxation of the MQ NMR coherences are in agreement with theoretical results. This means, in particular, that the relaxation of the MQ NMR coherences on the evolution period is determined by DDI.

Acknowledgements

This work is supported by the Russian Foundation for Basic Research (Grants No. 16-03-00056 and 19-32-80004) and the Program of the Presidium of RAS No. 5 "Electron spin resonance, spin-dependent electron effects and spin technologies". The experimental measurements were carried out using the equipment of the "Analytical center for collective use of IPCP RAS".

References

[1] M.A. Nielsen, I.L. Chuang, Quantum Computation and Quantum Information, Cambridge University Press, 2000.
[2] T.D. Ladd, D. Maryenko, Y. Yamamoto, E. Abe, K.M. Itoh, Coherence time of decoupled nuclear spins in silicon, Phys. Rev. B 71 (2005) 014401.
[3] D. Suter, T.S. Mahesh, Spins as qubits: quantum information processing by nuclear magnetic resonance, J. Chem. Phys. 128 (5) (2008) 052206.
[4] G.A. Álvarez, E.P. Danieli, P.R. Levstein, H.M. Pastawski, Decoherence as attenuation of mesoscopic echoes in a spin-chain channel, Phys. Rev. A 82 (2010) 012310.
[5] H.G. Krojanski, D. Suter, Decoherence in large NMR quantum registers, Phys. Rev. A 74 (2006) 062319.
[6] G. Kaur, A. Ajoy, P. Cappellaro, Decay of spin coherences in one-dimensional spin systems, New J. Phys. 15 (9) (2013) 093035.
[7] J. Baum, M. Munovitz, A.N. Garroway, A. Pines, Multiple quantum dynamics in solid state NMR, J. Chem. Phys. 83 (5) (1985) 2015–2025.
[8] H.G. Krojanski, D. Suter, Reduced decoherence in large quantum registers, Phys. Rev. Lett. 97 (2006) 150503.
[9] G.A. Bochkin, E.B. Fel'dman, S.G. Vasil'ev, V.I. Volkov, Dipolar relaxation of multiple quantum NMR coherences in one-dimensional systems, Chem. Phys. Lett. 680 (2017) 56–60.
[10] P. Cappellaro, Implementation of state transfer hamiltonians in spin chains with magnetic resonance techniques, in: G. Nikolopoulos, I. Jex (Eds.), Quantum State Transfer and Network Engineering, Springer, Berlin, Heidelberg, 2014, pp. 183–222.
[11] E.B. Fel'dman, A.N. Pyrkov, A.I. Zenchuk, Solid-state multiple quantum NMR in quantum information processing: exactly solvable models, Philos. Trans. Roy. Soc. A: Math. Phys. Eng. Sci. 370 (1976) (2012) 4690–4712.
[12] J.R. Goldman, T.D. Ladd, F. Yamaguchi, Y. Yamamoto, Magnet designs for a crystal-lattice quantum computer, Appl. Phys. A 71 (1) (2000) 11–17.
[13] K.M. Itoh, An all-silicon linear chain NMR quantum computer, Solid State Commun. 133 (11) (2005) 747–752.
[14] E.B. Fel'dman, S. Lacelle, Multiple quantum NMR spin dynamics in one-dimensional quantum spin chains, Chem. Phys. Lett. 253 (27) (1996) 27.
[15] E.B. Fel'dman, S. Lacelle, Multiple quantum nuclear magnetic resonance in one-dimensional quantum spin chains, J. Chem. Phys. 107 (18) (1997) 7067–7084.
[16] M. Munowitz, A. Pines, M. Mehring, Multiple-quantum dynamics in NMR: a directed walk through Liouville space, J. Chem. Phys. 86 (6) (1987) 3172–3182.
[17] W. van der Lugt, W.J. Caspers, Nuclear magnetic resonance line shape of fluorine in apatite, Physica 30 (8) (1964) 1658–1666.
[18] M. Engelsberg, I.J. Lowe, J.L. Carolan, Nuclear-magnetic-resonance line shape of a linear chain of spins, Phys. Rev. B 7 (1973) 924–929.
[19] A. Sur, I.J. Lowe, NMR line-shape calculation for a linear dipolar chain, Phys. Rev. B 12 (1975) 4597–4603.
[20] J.C. Elliott, Structure and chemistry of the apatites and other calcium orthophosphates, Studies in Inorganic Chemistry, vol. 18, Elsevier Science, Amsterdam, 1994.
[21] S.I. Doronin, I.I. Maksimov, E.B. Fel'dman, Multiple-quantum dynamics of one-dimensional nuclear spin systems in solids, J. Exp. Theor. Phys. 91 (3) (2000) 597–609.
[22] G. Cho, J.P. Yesinowski, Multiple-quantum NMR dynamics in the quasi-one-dimensional distribution of protons in hydroxyapatite, Chem. Phys. Lett. 205 (1) (1993) 1–5.
[23] L.B. Moran, J.P. Yesinowski, Chemical-shift-selective multiple-quantum NMR as a probe of the correlation length of chemical shielding tensors, Chem. Phys. Lett. 222 (4) (1994) 363–370.
[24] G. Cho, J.P. Yesinowski, ^{1}H and ^{19}F multiple-quantum NMR dynamics in quasi-one-dimensional spin clusters in apatites, J. Phys. Chem. 100 (39) (1996) 15716–15725.
[25] P. Cappellaro, C. Ramanathan, D.G. Cory, Simulations of information transport in spin chains, Phys. Rev. Lett. 99 (2007) 250506.
[26] S.I. Doronin, S.G. Vasil'ev, A.A. Samoilenko, E.B. Fel'dman, B.A. Shumm, Dynamics and relaxation of multiple quantum NMR coherences in a quasi-one-dimensional chain of nuclear spins ^{19}F in calcium fluorapatite, JETP Lett. 101 (9) (2015) 613–617.
[27] G.A. Bochkin, E.B. Fel'dman, S.G. Vasil'ev, V.I. Volkov, Dipolar relaxation of multiple quantum NMR coherences as a model of decoherence of many-qubit coherent clusters, Appl. Magn. Reson. 49 (1) (2018) 25–34.
[28] G.A. Bochkin, E.B. Fel'dman, S.G. Vasil'ev, Relaxation of multiple quantum NMR coherences in quasi-one-dimensional spin systems, Z. Phys. Chem. 231 (3) (2017) 513–525.
[29] S.I. Doronin, E.B. Fel'dman, I.I. Maksimov, Line shapes of multiple quantum NMR coherences in one-dimensional quantum spin chains in solids, J. Magn. Reson. 171 (2004) 37–42.
[30] V.E. Zobov, A.A. Lundin, Decay of multispin multiquantum coherent states in the NMR of a solid, J. Exp. Theor. Phys. 112 (3) (2011) 451–459.
[31] V.E. Zobov, A.A. Lundin, Decay of multispin multiple-quantum coherent states in the NMR of a solid and the stabilization of their intensity profile with time, J. Exp. Theor. Phys. 113 (6) (2011) 1006–1014.
[32] U. Haeberlen, High Resolution NMR in Solids: Selective Averaging, Academic Press, 1976.
[33] W-K. Rhim, A. Pines, J.S. Waugh, Time-reversal experiments in dipolar-coupled spin systems, Phys. Rev. B 3 (1971) 684–696.
[34] W. Zhang, P. Cappellaro, N. Antler, B. Pepper, D.G. Cory, V.V. Dobrovitski, C. Ramanathan, L. Viola, NMR multiple quantum coherences in quasi-one-dimensional spin systems: comparison with ideal spin-chain dynamics, Phys. Rev. A 80 (2009) 052323.
[35] Y.-S. Yen, A. Pines, Multiple-quantum NMR in solids, J. Chem. Phys. 78 (6) (1983) 3579–3582.
[36] K. Momma, F. Izumi, VESTA 3 for three-dimensional visualization of crystal, volumetric and morphology data, J. Appl. Crystallogr. 44 (6) (2011) 1272–1276.
[37] J.L. Carolan, A pulsed NMR investigation of ^{19}F chemical shift anisotropy in single crystals of fluorapatite, Chem. Phys. Lett. 12 (2) (1971) 389–391.
[38] G. Cho, C.-N. Chau, J.P. Yesinowski, ^{19}F MAS NMR investigation of strontium substitution sites in Ca^{2+}/Sr^{2+} fluorapatite solid solutions, J. Phys. Chem. C 112 (15) (2008) 6165–6172.
[39] J.P. Yesinowski, Nuclear magnetic resonance spectroscopy of calcium phosphates, in: Z. Amjad (Ed.), Calcium Phosphates in Biological and Industrial Systems, Springer US, Boston, MA, 1998, pp. 103–143, Chapter 6.

[40] E.R. Andrew, D.P. Tunstall, Anisotropy of chemical shift for some fluorine compounds, Proc. Phys. Soc. 81 (6) (1963) 986.
[41] M. Braun, P. Hartmann, C. Jana, ^{19}F and ^{31}P NMR spectroscopy of calcium apatites, J. Mater. Sci. Mater. Med. 6 (3) (1995) 150–154.
[42] G.E. Pake, Nuclear resonance absorption in hydrated crystals: fine structure of the proton line, J. Chem. Phys. 16 (4) (1948) 327–336.
[43] G. Kaur, P. Cappellaro, Initialization and readout of spin chains for quantum information transport, New J. Phys. 14 (8) (2012) 083005.
[44] D.H. Levy, K.K. Gleason, Multiple quantum nuclear magnetic resonance as a probe for the dimensionality of hydrogen in polycrystalline powders and diamond films, J. Phys. Chem. 96 (20) (1992) 8125–8131.
[45] A.K. Khitrin, Growth of NMR multiple-quantum coherences in quasi-one-dimensional systems, Chem. Phys. Lett. 274 (1) (1997) 217–220.
[46] D.N. Shykind, J. Baum, S.-B. Liu, A. Pines, A.N. Garroway, Phase-incremented multiple-quantum NMR experiments, J. Magn. Reson. 76 (1) (1988) 149–154.
[47] O.N. Antzutkin, R. Tycko, High-order multiple quantum excitation in ^{13}C nuclear magnetic resonance spectroscopy of organic solids, J. Chem. Phys. 110 (6) (1999) 2749–2752.
[48] K. Saalwächter, P. Ziegler, O. Spyckerelle, B. Haidar, A. Vidal, J.-U. Sommer, ^{1}H multiple-quantum nuclear magnetic resonance investigations of molecular order distributions in poly(dimethylsiloxane) networks: evidence for a linear mixing law in bimodal systems, J. Chem. Phys. 119 (6) (2003) 3468–3482.
[49] W. van der Lugt, D.I.M. Knottnerus, W.G. Perdok, Nuclear magnetic resonance investigation of fluoride ions in hydroxyapatite, Acta Crystallogr. B 27 (8) (1971) 1509–1516.
[50] A.M. Vakhrameev, S.P. Gabuda, R.G. Knubovets, ^{1}H and ^{19}F NMR in apatites of the type $Ca_5(PO_4)_3[F_{1-x}(OH)_x]$, J. Struct. Chem. 27 (8) (1971) 1509–1516.
[51] G.A. Bochkin, S. G Vasil'ev, I.D. Lazarev, E.B. Fel'dman, The second moments of the line shapes of multiple quantum NMR coherences in one-dimensional systems, J. Exp. Theor. Phys. 127 (3) (2018) 532–538.